J|A|C|S ARTICLES

Published on Web 10/06/2009

Design, Synthesis, and Testing of Difluoroboron-Derivatized Curcumins as Near-Infrared Probes for in Vivo Detection of Amyloid-β Deposits

Chongzhao Ran,[†] Xiaoyin Xu,[‡] Scott B. Raymond,[§] Brian J. Ferrara,[§] Krista Neal,[§] Brian J. Bacskai,[§] Zdravka Medarova,[†] and Anna Moore*[,†]

Molecular Imaging Laboratory, MGH/MIT/HMS Athinoula A. Martinos Center for Biomedical Imaging, Department of Radiology, Massachusetts General Hospital/Harvard Medical School, Room 2301, Building 149, Charlestown, Massachusetts 02129, Optical Imaging Laboratory, Department of Radiology, Brigham and Women's, Hospital, Boston, Massachusetts 02115, and Alzheimer's Disease Research Unit, Department of Neurology, Massachusetts General Hospital, Boston, Massachusetts 02114

Received June 16, 2009; E-mail: amoore@helix.mgh.harvard.edu

Abstract: Amyloid-β (Aβ) deposits have been identified as key players in the progression of Alzheimer's disease (AD). Recent evidence indicates that the deposits probably precede and induce the neuronal atrophy. Therefore, methods that enable monitoring the pathology before clinical symptoms are observed would be beneficial for early AD detection. Here, we report the design, synthesis, and testing of a curcumin-derivatized near-infrared (NIR) probe, CRANAD-2. Upon interacting with Aβ aggregates, CRANAD-2 undergoes a range of changes, which include a 70-fold fluorescence intensity increase, a 90 nm blue shift (from 805 to 715 nm), and a large increase in quantum yield. Moreover, this probe also shows a high affinity for Aβ aggregates (K_d = 38.0 nM), a reasonable log P value (log P = 3), considerable stability in serum, and a weak interaction with albumin. After intravenous injection of this probe, 19-month-old Tg2576 mice exhibited significantly higher relative signal than that of the control mice over the same period of time. In summary, CRANAD-2 meets all the requirements for a NIR contrast agent for the detection of Aβ plaques both in vitro and in vivo. Our data point toward the feasibility of monitoring the progress of the disease by NIR imaging with CRANAD-2. In addition, we believe that our probe could be potentially used as a tool for drug screening.

Introduction

Amyloid-β (Aβ) deposits are a pathological hallmark of Alzheimer's disease (AD). Their formation arises from the aggregation of peptides Aβ40 and Aβ42, which are generated from amyloid peptide precursor (APP) by cleavage with β- and γ-secretases.[1] Although the assertion that Aβ deposits precede and induce neuronal atrophy remains controversial,[2] recent evidence indicates that Aβ plaques are a critical mediator of neuritic pathology.[3] Currently, memory and behavioral tests are widely used for late-stage AD diagnosis;[4] however, early detection at the asymptomatic syndrome stage still presents a challenge. Molecular imaging, a detection technique with sensitivity at the molecular level, represents a promising approach to face this challenge. Magnetic resonance imaging (MRI), positron emission tomography (PET), and optical imaging have each been employed for the early detection of AD pathology, and considerable progress has been achieved in recent years.[5−13] Although studies indicate that molecular MRI is a promising diagnostic modality, its low sensitivity could be an obstacle for its application in the clinic. In recent years, it has been demonstrated that PET can also be used as a powerful imaging modality to detect AD pathology; however, its high

[†] Department of Radiology, Massachusetts General Hospital/Harvard Medical School.
[‡] Department of Radiology, Brigham and Women's Hospital.
[§] Department of Neurology, Massachusetts General Hospital.

(1) Selkoe, D. J. *Nature* **1999**, *399*, A23–31.
(2) Stokin, G. B.; Lillo, C.; Falzone, T. L.; Brusch, R. G.; Rockenstein, E.; Mount, S. L.; Raman, R.; Davies, P.; Masliah, E.; Williams, D. S.; Goldstein, L. S. *Science* **2005**, *307*, 1282–8.
(3) Meyer-Luehmann, M.; Spires-Jones, T. L.; Prada, C.; Garcia-Alloza, M.; de Calignon, A.; Rozkalne, A.; Koenigsknecht-Talboo, J.; Holtzman, D. M.; Bacskai, B. J.; Hyman, B. T. *Nature* **2008**, *451*, 720–4.
(4) Dubois, B.; et al. *Lancet Neurol.* **2007**, *6*, 734–46.
(5) Klunk, W.; et al. *Ann. Neurol.* **2004**, *55*, 306–19.
(6) Hintersteiner, M.; Enz, A.; Frey, P.; Jaton, A. L.; Kinzy, W.; Kneuer, R.; Neumann, U.; Rudin, M.; Staufenbiel, M.; Stoeckli, M.; Wiederhold, K. H.; Gremlich, H. U. *Nat. Biotechnol.* **2005**, *23*, 577–83.
(7) Skovronsky, D. M.; Zhang, B.; Kung, M. P.; Kung, H. F.; Trojanowski, J. Q.; Lee, V. M. *Proc. Natl. Acad. Sci. U.S.A.* **2000**, *97*, 7609–14.
(8) Nesterov, E. E.; Skoch, J.; Hyman, B. T.; Klunk, W. E.; Bacskai, B. J.; Swager, T. M. *Angew. Chem., Int. Ed. Engl.* **2005**, *44*, 5452–6.
(9) Higuchi, M.; Iwata, N.; Matsuba, Y.; Sato, K.; Sasamoto, K.; Saido, T. C. *Nat. Neurosci.* **2005**, *8*, 527–33.
(10) Poduslo, J. F.; Curran, G. L.; Peterson, J. A.; McCormick, D. J.; Fauq, A. H.; Khan, M. A.; Wengenack, T. M. *Biochemistry* **2004**, *43*, 6064–75.
(11) Jack, C. R., Jr.; Garwood, M.; Wengenack, T. M.; Borowski, B.; Curran, G. L.; Lin, J.; Adriany, G.; Grohn, O. H.; Grimm, R.; Poduslo, J. F. *Magn. Reson. Med.* **2004**, *52*, 1263–71.
(12) Lee, V. M. *Proc. Natl. Acad. Sci. U.S.A.* **2001**, *98*, 8931–2.
(13) Wadghiri, Y. Z.; Sigurdsson, E. M.; Sadowski, M.; Elliott, J. I.; Li, Y.; Scholtzova, H.; Tang, C. Y.; Aguinaldo, G.; Pappolla, M.; Duff, K.; Wisniewski, T.; Turnbull, D. H. *Magn. Reson. Med.* **2003**, *50*, 293–302.

cost and the narrow isotope availability of PET probes limit its broad usage.[5] Molecular optical imaging, including multiphoton and near-infrared imaging, has been used to detect early AD pathology in animal models. The invasiveness and small field-of-view of multiphoton imaging limit its application, and this approach is not translatable for clinical imaging.[5,8,14−16] Near-infrared imaging (NIR) is an attractive tool for early AD detection because of its acceptable depth penetration, noninvasive operation, and inexpensive instrumentation. Though NIR imaging is so far limited to animal studies, some NIR probes could be easily modified to PET imaging probes and thus are worth pursuing. In addition, new optical imaging systems such as fluorescent molecular tomographic (FMT) imaging are being developed for clinical applications.[17] While several non-NIR molecules that specifically bind to senile plaques have been reported for multiphoton imaging and histological studies,[5,14,18] only a few near-infrared probes have been reported thus far.[6,8,19]

In principle, a good NIR probe for senile plaques should have the following properties:[5,8] (1) specificity to Aβ plaques, (2) reasonable lipophilicity (log P between 1 and 3), (3) molecular mass less than 600 Da, (4) emission wavelength >650 nm and a large Stokes shift, (5) high-affinity binding, (6) high quantum yield, (7) low-affinity binding with bovine serum albumin (BSA), (8) reasonable stability in blood, (9) straightforward synthesis, and most importantly, (10) upon binding to Aβ plaques, it should significantly change its fluorescence properties (i.e., fluorescence intensity, fluorescence lifetime, emission wavelength, and quantum yield). An increase in fluorescence intensity means that the probe will be "turned on" upon interacting with a target. To date, none of the reported NIR probes meet all of these criteria. Although the oxazine-derivative probe AOI 987 was reported as an efficient NIR probe for detecting and monitoring senile plaques, it has a small Stokes shift (25 nm) and moderate binding ($K_d = 220$ nM).[6] Moreover, it displayed a slight fluorescence intensity decrease instead of significant fluorescence intensity increase upon binding with Aβ aggregates. NIAD-4 was reported as a senile plaque-specific probe for two-photon microscopy and could be used as a NIR probe as well.[8] Additionally, Li et al.[18] reported that some styryl dyes could be "turned on" upon incubation with Aβ aggregates, but these compounds may have little chance of penetrating the blood brain barrier (BBB) because of their high polarity.

Curcumin, a brightly colored powder, is the principal curcuminoid of Indian curry and has been consumed daily for thousands of years in India and other regions. Curcumin is known for its antitumor, antioxidant, antiarthritic, and anti-inflammatory properties.[20−23] It has been utilized as an anti-amyloid agent as well.[14,24] In 2005, Yang et al.[24] reported that curcumin could be used as a histological staining reagent for senile plaques and showed that curcumin could decrease amyloid deposits in vivo. Further, Garcia-Alloza et al.[14] demonstrated by two-photon imaging that curcumin could be visualized in vivo and could prevent the progress of amyloid plaque formation in APP-τ transgenic mouse model. In addition, Ryu et al.[25] suggested that curcumin derivatives were potential PET probes for amyloid imaging. All of the studies demonstrate that curcumin has some specificity for amyloid plaques and displays high-affinity binding for Aβ aggregates ($K_d = 0.20$ nM).[25] However, curcumin is not a practical probe for in vivo NIR imaging because of its short emission wavelength, limited access across the blood−brain barrier, and rapid metabolism.[25] Despite these limitations, we hypothesized that, by modifying the structure of curcumin, it would be possible to shift the emission wavelength to the NIR range and create a probe with significant changes in fluorescence properties upon binding to plaques that had a better pharmacokinetic profile and was less susceptible to metabolic degradation. Here we report on the design, synthesis, and testing of curcumin derivatives as NIR imaging probes that meet all of the above-mentioned criteria.

Results and Discussion

Design, Synthesis, and Spectra of Probes. The rationale behind the design of our NIR probe was based on three facts. First, it is a known phenomenon that curcumin reacts with boric acid to form a red compound, rosocyanine, which consists of two curcumins connected by a borate ring.[26,27] The color change from yellow (curcumin) to red (rosocyanine) indicates an absorption red shift, which may be ascribed to the introduction of a boron atom ($\pi \rightarrow \pi^*$ from oxygen to empty orbital of boron) into the rosocyanine molecule. We hypothesized that we could utilize the red shift benefit of boron incorporation to design boron-containing curcumin derivatives with emission in the 650−900 nm range. Second, although 2,2-difluoro-1,3,2-dioxaborines are known compounds and their fluorescence properties have been characterized,[28−32] the fluorescence change caused by difluoroboronate incorporation into diketone remains unclear. Nonetheless, introduction of a difluoroboronate ring into dipyrromethene systems forms well-documented red-shifted Bodipy dyes.[33] Therefore, it was reasonable to speculate that, by incorporating a difluoroboronate moiety into curcumin, it

(14) Garcia-Alloza, M.; Borrelli, L. A.; Rozkalne, A.; Hyman, B. T.; Bacskai, B. J. *J. Neurochem.* **2007**, *102*, 1095–104.
(15) Bacskai, B. J.; Frosch, M. P.; Freeman, S. H.; Raymond, S. B.; Augustinack, J. C.; Johnson, K. A.; Irizarry, M. C.; Klunk, W. E.; Mathis, C. A.; Dekosky, S. T.; Greenberg, S. M.; Hyman, B. T.; Growdon, J. H. *Arch. Neurol.* **2007**, *64*, 431–4.
(16) D'Amore, J. D.; Kajdasz, S. T.; McLellan, M. E.; Bacskai, B. J.; Stern, E. A.; Hyman, B. T. *J. Neuropathol. Exp. Neurol.* **2003**, *62*, 137–45.
(17) Weissleder, R.; Pittet, M. *Nature* **2008**, *452*, 580–9.
(18) Li, Q.; Lee, J. S.; Ha, C.; Park, C. B.; Yang, G.; Gan, W. B.; Chang, Y. T. *Angew. Chem., Int. Ed.* **2004**, *43*, 6331–5.
(19) Raymond, S. B.; Skoch, J.; Hills, I. D.; Nesterov, E. E.; Swager, T. M.; Bacskai, B. J. *Eur. J. Nucl. Med. Mol. Imaging* **2008**, *35* (Suppl. 1), S93–8.
(20) Shishodia, S.; Sethi, G.; Aggarwal, B. B. *Ann. N.Y. Acad. Sci.* **2005**, *1056*, 206–17.
(21) Siwak, D. R.; Shishodia, S.; Aggarwal, B. B.; Kurzrock, R. *Cancer* **2005**, *104*, 879–90.
(22) Aggarwal, B. B.; Shishodia, S.; Takada, Y.; Banerjee, S.; Newman, R. A.; Bueso-Ramos, C. E.; Price, J. E. *Clin. Cancer Res.* **2005**, *11*, 7490–8.
(23) Aggarwal, S.; Ichikawa, H.; Takada, Y.; Sandur, S. K.; Shishodia, S.; Aggarwal, B. B. *Mol. Pharmacol.* **2006**, *69*, 195–206.
(24) Yang, F.; Lim, G. P.; Begum, A. N.; Ubeda, O. J.; Simmons, M. R.; Ambegaokar, S. S.; Chen, P. P.; Kayed, R.; Glabe, C. G.; Frautschy, S. A.; Cole, G. M. *J. Biol. Chem.* **2005**, *280*, 5892–901.
(25) Ryu, E. K.; Choe, Y. S.; Lee, K. H.; Choi, Y.; Kim, B. T. *J. Med. Chem.* **2006**, *49*, 6111–9.
(26) Roth, H. J.; Miller, B. *Arch. Pharm. (Weinheim)* **1964**, *297*, 617–23.
(27) Roth, H. J.; Miller, B. *Arch. Pharm. Ber. Dtsch. Pharm. Ges.* **1964**, *297*, 660–73.
(28) Zhang, G.; Chen, J.; Payne, S. J.; Kooi, S. E.; Demas, J. N.; Fraser, C. L. *J. Am. Chem. Soc.* **2007**, *129*, 8942–3.
(29) Hales, J. M.; Zheng, S.; Barlow, S.; Marder, S. R.; Perry, J. W. *J. Am. Chem. Soc.* **2006**, *128*, 11362–3.
(30) Chow, Y. L.; Johansson, C. I. *J. Phys. Chem.* **1995**, *99*, 17558–65.
(31) Cogné-Laage, E.; Allemand, J.-F.; Ruel, O.; Baudin, J.-B.; Croquette, V.; Blanchard-Desce, M.; Jullien, L. *Chem.—Eur. J.* **2004**, *10*, 1445–55.
(32) Pfister, A.; Zhang, G.; Zareno, J.; Horwitz, A. F.; Fraser, C. L. *ACS Nano* **2008**, *2*, 1252–8.
(33) Ulrich, G.; Ziessel, R.; Harriman, A. *Angew. Chem., Int. Ed. Engl.* **2008**, *47*, 1184–201.

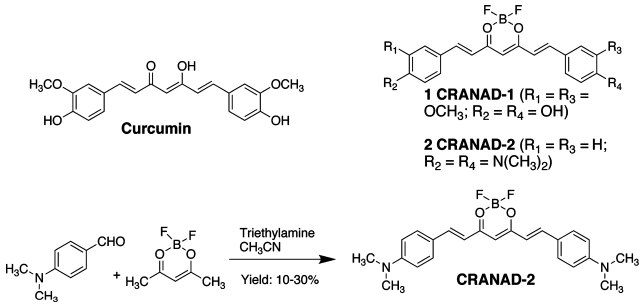

Figure 1. (Top) Structure of curcumin, compound **1** (CRANAD-1), and compound **2** (CRANAD-2); (bottom) synthetic route for CRANAD-2. NMR spectra for CRANAD-2 are shown in Figure 2 in Supporting Information.

would generate an appropriate red shift. Finally, the *N*,*N*′-dimethyl group is well-known as the best absorption red-shift pushing group for para-substituted aromatic rings.[34] We accordingly further proposed to modify curcumin by replacing the phenolic hydroxyl groups with *N*,*N*′-dimethyl groups to enable red-shifted absorption and consequently lead to an additional red shift in emission (Figure 1). On the basis of these considerations, probes **1** and **2** were designed and synthesized. Compound **1** has been reported as an HIV-1 and HIV-2 protease inhibitor,[35] and this probe was synthesized by following the reported procedure.[35,36] Compound **2** was prepared by condensation of 4-*N*,*N*′-dimethylbenzaldehyde with 2,2-difluoro-1,3-dioxaboryl-pentadione in acetonitrile.[29] For convenience, in the proceedings of this report, we named compound **1** as CRANAD-1 and compound **2** as CRANAD-2 (which stands for the initial and last name of the first author, C. Ran, as well as for Alzheimer's disease, AD).

As anticipated, there was an approximately 80 nm red shift of emission after installation of the difluoroboron ring into the curcumin molecule (CRANAD-1). In methanol, the maximum emission of CRANAD-1 was 640 nm, while the $\lambda_{max(em)}$ of curcumin was 560 nm (Figure 1A in Supporting Information). There was also a 100 nm Stokes shift for CRANAD-1 [$\lambda_{max(ex)} = 540$ nm, $\lambda_{max(em)} = 640$ nm], which was larger than that of curcumin's 50 nm shift [$\lambda_{max(ex)} = 510$ nm, $\lambda_{max(em)} = 560$ nm] (data not shown). Although we achieved considerable red shift and Stokes shift with CRANAD-1, our ultimate goal was to push the emission further into NIR range. In order to do this we further modified CRANAD-1 by replacing the phenolic hydroxyl group with *N*,*N*′-dimethyl group to yield compound CRANAD-2.

With this replacement, the emission of CRANAD-2 was red-shifted to $\lambda_{max(em)} = 760$ nm in methanol, which falls in the best range for NIR probes. The compound also displayed a large Stokes shift [$\lambda_{max(ex)} = 640$ nm, $\lambda_{max(em)} = 805$ nm] (Figure 1B in Supporting Information) in phosphate-buffered saline (PBS). Furthermore, by comparison with the fluorescence intensity in methanol, the quantum yield of CRANAD-2 was significantly higher than that of curcumin (Figure 1A in Supporting Information). As expected, the emission wavelength of CRANAD-2 displayed a typical solvent dependency (Figure 1C in Supporting Information); that is, it showed longer emission and lower

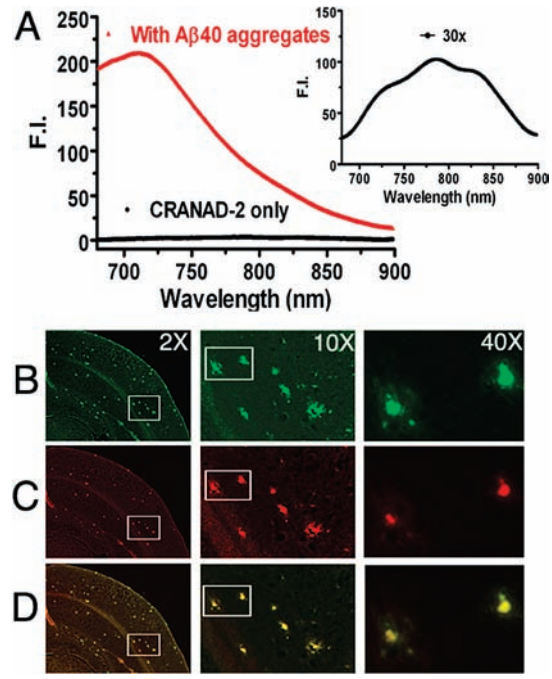

Figure 2. (A) Fluorescence "turn on" of CRANAD-2 (100 nM) induced by Aβ aggregates (red line); CRANAD-2 alone in PBS (black line); (inset) CRANAD-2 only (emission intensity is amplified 30-fold). (B−D) Histological staining of the brain slices from an APP-PS1 transgenic mouse. Magnification: left, 2×; middle, 10× (region highlighted in left panel); right, 40× (region highlighted in middle panel). (B) Staining with thioflavin T indicated abundant plaques in the cortex region. (C) Staining with CRANAD-2. (D) Merged images of B and C.

quantum yield in polar solvent. Taken together, we demonstrated that, by two-step red-shift modification of curcumin, we were able to push its emission wavelength into an ideal emission range for NIR probes. Additionally, these modifications produced a large Stokes shift of CRANAD-2.

In Vitro Test with CRANAD-2. We tested the binding affinity and fluorescence intensities of CRANAD-2 with synthetic Aβ(1−40) aggregates in PBS (pH 7.4). While we observed weak fluorescence intensity for the probe alone in PBS, there was a remarkable 70-fold fluorescence intensity increase in the presence of Aβ40 aggregates (Figure 2A). This result suggested that our probe could be "turned on" upon interacting with its substrate. This was further reflected by the changes in quantum yield from 0.006 in PBS to 0.40 after binding to Aβ40 aggregates. A significant blue shift (from 805 to 715 nm, total shift of 90 nm, inset in Figure 2A) was observed as well after binding with Aβ40 aggregates, possibly indicating the insertion of the dye into the hydrophobic environment of the aggregates. Taken together, CRANAD-2, upon binding to Aβ40 aggregates, displayed a "turn on" phenomenon, a quantum yield increase, and a considerable emission blue shift.

Next, the apparent binding constant ($K_d = 38.69 \pm 2.77$ nM, $R_2 = 0.9952$, Figure 3 in Supporting Information) of CRANAD-2 to Aβ aggregates was measured by fluorescence intensity (FI) with various concentrations of the probe. This binding constant was significantly higher than that of thioflavin T, a widely used agent for detecting protein and peptide aggregation such as Aβ aggregation ($K_d = 580$ nM);[37] higher than that of AOI 987 ($K_d = 220 \pm 130$ nM);[6] close to that of

(34) *Organic Structure Analysis*; Crews, P., Rodriguez, J., Jaspars, M., Eds.; Oxford University Press: New York, 1998.
(35) Zhao, H.; Neamati, N.; Hong, H.; Mazumder, A.; Wang, S.; Sunder, S.; Milne, G. W.; Pommier, Y.; Burke, T. R., Jr. *J. Med. Chem.* **1997**, *40*, 242–9.
(36) Weber, W. M.; Hunsaker, L. A.; Abcouwer, S. F.; Deck, L. M.; Vander Jagt, D. L. *Bioorg. Med. Chem.* **2005**, *13*, 3811–20.
(37) Klunk, W. E.; Wang, Y.; Huang, G. F.; Debnath, M. L.; Holt, D. P.; Mathis, C. A. *Life Sci.* **2001**, *69*, 1471–84.

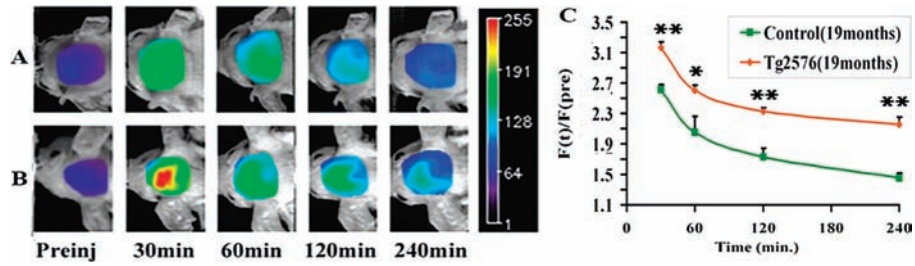

Figure 3. Representative images of Tg2576 mice and control littermates at different time points before and after iv injection of 5.0 mg/kg CRANAD-2. (A) A 19-month old control mouse; (B) 19-month-old Tg2576 mouse (mice showed similar background fluorescence signal). (C) The relative fluorescence signal $[F_{(t)}/F_{(pre)}]$ was significantly higher than that of the control mice, and the decay of fluorescence signal was significantly slower in transgenic mice compared to the control group ($*p \leq 0.05$, $**p \leq 0.01$).

NIAD-4 (K_d = 10.0 nM);[8] and lower than that of PiB (K_d = 4.7 nM), a PET probe under international clinic trials for Aβ deposits imaging.[5] We found no significant change in fluorescence during incubation with BSA (Figure 4 in Supporting Information), suggesting that there is little or no interaction between the probe and BSA. Furthermore, we also found that the probe was stable when CRANAD-2 was incubated in human serum for 2 h at 37 °C. Both fluorescence and HPLC spectra showed about 70% recovery of the probe, indicating its relative stability (Figure 5A−D in Supporting Information). Additionally, we confirmed the capability of CRANAD-2 to detect Aβ plaques in vitro by staining brain sections from a 12-month-old APP-PS1 transgenic mouse. We observed high-contrast staining of plaques in the tissue, which colocalized with the signal from standard thioflavin T-stained sections (Figure 2B−D). These results indicate CRANAD-2's specificity for Aβ plaques.

Blood−Brain Barrier Penetrating Test of CRANAD-2. In order for the probe to cross the blood−brain barrier, its lipophilicity (log *P*) should be within the 1−3 range. Our testing of the lipophilicity of CRANAD-2 resulted in a log *P* = 3.0, indicating that CRANAD-2 holds promise as a BBB penetrating probe. To further demonstrate the probe's BBB penetrating ability, we intravenously injected wild-type mice with CRANAD-2 and measured the concentration of the dye in plasma and brain at a range of time points postmortem. PiB, a well-studied plaque-specific PET probe, was used as a positive control,[5] while ICG, a known non-BBB penetrating probe, was used as a negative control. As shown in Figure 6 in Supporting Information, both the fluorescence spectrum and HPLC analysis of the brain homogenate confirmed the presence of CRANAD-2 in the brain (Figure 6B−D in Supporting Information). CRANAD-2 displayed rapid clearance from blood while clearance from the brain was significantly slower. Compared to PiB, CRANAD-2 showed less entry into brain and slower clearance. There was no detectable ICG in brain homogenates after intravenous (iv) injection at all time points (Figure 6A in Supporting Information).

In Vivo Imaging and ex Vivo Histology. To validate the feasibility of CRANAD-2 as a NIR imaging probe, transgenic 19-month-old Tg2576 mice were used, and age-matched wild-type littermates served as controls. Tg2576 transgenic mouse model, also known as APPswe mouse model, carries a transgene coding for the 695 amino acid isoform of human Alzheimer β-amyloid (Aβ) precursor protein (APP) and expresses high concentrations of the mutant Aβ. It develops significant amyloid plaques and displays memory deficits around 10−12 months of age.[38] Tg2576 mice have been widely used in the AD research community. In this study, we used fluorescence intensity-based NIR imaging technique to capture mice images. For this technology, fluorescence reflectance (also known as epifluorescence) and tomography (FMT) are the two most used modalities for in vivo small animal imaging. Reflectance imaging is suitable for fast imaging but has less penetrating depth (<1 cm) and poor resolution. Although FMT has better resolution and deeper penetrating ability (<10 cm),[17] it is still in the development stage. Therefore, we chose the reflectance imaging technique to conduct the in vivo imaging. Mice images were recorded before and after iv injection of CRANAD-2 at 5.0 mg/kg dosage. For mice with comparable background fluorescence (F_{pre}) (Figure 3, A vs B), the fluorescence signal diminished considerably more slowly for 19-month-old Tg2576 mice than for the control group. Fluorescence intensities of the transgenic group were higher than those of the control group at 30, 60, 120, and 240 min. These results were correlated to semiquantitative analysis of the images, which was performed by selecting a region of interest (ROI) in the brain and normalizing fluorescence intensity at any given time point $[F_{(t)}]$ to background fluorescence intensity before the injection $[F_{(pre)}]$. For Tg2576 and control mice, the differences of normalized signal were 55%, 68%, 61%, and 70% at 30, 60, 120, and 240 min, respectively. Notably, our data showed that the differences between transgenic and control groups could be observed at the earliest time point (30 min.). Finally, we confirmed the presence of CRANAD-2 by ex vivo histology. Mice were intravenously injected with 5.0 mg/kg CRANAD-2 probe, perfused, and sacrificed 2 h after injection. We observed senile plaques in brain slices from 19-month-old transgenic mice. However, there were no plaques found in the age-matched littermates (Figure 7 in Supporting Information). These results further confirmed our in vivo imaging data that the CRANAD-2 probe could penetrate the BBB and label senile plaques specifically in vivo.

Experimental Section

General materials and methods are available in the Supporting Information. Synthetic amyloid-β peptide(1−40) was purchased from rPeptide (Bogart, GA) and aggregates for in vitro studies were generated followed the reported procedure.[37,39] Transgenic Tg2576 mice[38] and littermates were purchased from Taconic Farm, Balb/c mice for BBB penetrating test were obtained from Jackson Laboratory, and the experiment procedure was approved by Massachusetts General Hospital. In vivo imaging was recorded on Kodak Imaging Station 2000MM.

Synthesis of CRANAD-1. The synthesis of CRANAD-1 was performed according to the reported procedure.[36]

(38) Hsiao, K.; Chapman, P.; Nilsen, S.; Eckman, C.; Harigaya, Y.; Younkin, S.; Yang, F.; Cole, G. *Science* **1996**, *274*, 99–102.
(39) Jun, S.; Saxena, S. *Angew. Chem., Int. Ed.* **2007**, *46*, 3959–61.

Synthesis of CRANAD-2. 2,2-Difluoro-1,3-dioxaborylpentadione was synthesized by a modified procedure.[29] 1,3-Pentadione (0.1 g, 1.0 mmol) and trifluoroboron ether (0.2 g, 1.0 mmol) were mixed together, and the resulting solution was heated at 60 °C for 2 h.. After cooling to room temperature, the reaction mixture was subjected to evaporation under vacuum, and a pale yellow semisolid was obtained, which was solidified with longer standing at room temperature to give pale yellow needle crystals. The above crystals (0.15 g, 0.1 mmol) were dissolved in acetonitrile (3.0 mL), followed by addition of triethylamine (0.30 g, 3.0 mmol) and 4-*N*,*N*′-dimethylbenzaldehyde (0.30 g, 2.0 mmol). The resultant was stirred at 60 °C overnight. A black residue was obtained after removal of the solvent and was subjected to flash column chromatography with methylene chloride to give a black powder (63.0 mg, yield 15.0%). ^{1}H NMR (DMSO-d_6) δ (ppm) 3.04 (s, 12H), 6.26 (s, 1H), 6.79 (m, 6H), 7.68 (d, 4H, $J = 8.0$ Hz), 7.82 (d, 2H, $J = 16$ Hz); ^{13}C NMR (DMSO-d_6) δ (ppm) 40.3, 101.0, 111.5, 112.5, 115.1, 122.2, 132.2, 146.5, 153.3, 177.3; ^{19}F NMR (DMSO-d_6) δ (ppm) −138.9; *m*/*z* 433 (M + Na).

In Vitro Aβ Aggregates Binding Constant Measurement. To PBS solutions (1.0 mL) of Aβ40 aggregates (5.0 μM, calculation based on Aβ40 peptide concentration), various amounts of CRANAD-2 were added to final concentrations of 2.5, 5.0, 10.0, 20.0, 40.0, 60.0, 100.0 150.0, 200.0, 250.0, and 300.0 nM, and their fluorescence intensities at 715 nm were recorded (Ex: 640 nm). The K_d binding curve was generated by software Prism 3.0 with nonlinear one-site binding regression. By measuring the fluorescence intensity of CRANAD-2 alone in PBS buffer (50.0, 100.0, 350.0, 850.0, and 1200.0 nM), we confirmed that there was no self-quenching of the dye within the range of the above tested concentrations.

In Vivo Near-Infrared Imaging. In vivo NIR imaging was performed on a Kodak Imaging station 2000MM. For fluorescence excitation, three laser diodes at 660 nm with a total power of 10 mW/cm^2 have been used, yielding uniform illumination of the whole animal. The fluorescent light emitted from the sample (mouse) was detected by a charge-coupled device (CCD) camera (Hamamatsu ORCA) equipped with a focusing lens system (macro lens 60 mm, 1:2.8, Nikon). The image matrix comprised 532 × 256 pixels. A bandpass filter was used for the selection of the detection wavelength (700 nm). Integration time default was selected at 30 s. Images were acquired with Kodak 1DTM 3.6.3 Network software and analyzed by use of the KodakTM 1D Analysis software.

Mice ($n = 3$ for Tg2576 and $n = 3$ for the littermates) were shaved before background imaging, and were iv injected with CRANAD-2 (5.0 mg/kg, 20% dimethyl sulfoxide (DMSO), 80% propylene glycol). Fluorescence signals from the brain were recorded preinjection and at 30, 60, 120, and 240 min after intravenous injection of the probe. To evaluate our imaging results, an ROI was drawn around the brain region. The data were analyzed by normalizing fluorescence intensity to background fluorescence of each mouse [i.e., $F_{(t)}/F_{(\mathrm{pre})}$], where $F_{(t)}$ is the fluorescence intensity of the time point of interest and $F_{(\mathrm{pre})}$ is the background fluorescence signal. *P* values were calculated by Student test.

Ex Vivo Histological Correlation. Nineteen-month-old mice and corresponding littermates were injected with CRANAD-2 (5.0 mg/kg), sacrificed at 120 min after injection, and perfused with 4% formaldehyde. The brains were excised and embedded in optimum cutting temperature compound (OCT). For microscopy, the brains were sliced into 25 μm slices, and each slice was equilibrated for 5 min and covered with VectaShield mounting media.

Conclusion

In this study we report on the design, synthesis, and testing of a novel NIR Aβ plaque-specific fluorescent probe, CRANAD-2. This probe is the first example of difluoroborate diketone compounds for in vivo biological studies, which provides a new type of NIR fluorescent dye for cell, tissue, and in vivo imaging for small animals. The new probe meets the requirements of a NIR probe for detecting Aβ deposits noninvasively in vivo. Currently, investigation of the feasibility of the probe for longitudinal monitoring of low molecular weight Aβ species (such as oligomers, prefibrillar, and fibrils) in vivo is underway. Because CRANAD-2 enters the brain and binds to amyloid plaques specifically, a radiolabeled version would be suitable for PET imaging. In addition, because of the promise of curcumin as a treatment for AD, we believe that CRANAD-2 might have therapeutic potential for this and other diseases.

Acknowledgment. This work was partially supported by the NIH Program Project Grants AG026240 (B.J.B.) and CA113672 (A.M.).

Supporting Information Available: General materials and methods, including log *P* measurement, stability test in serum, BSA interaction, and histological evaluation; complete refs 4 and 5; and seven figures as described in the text. This material is available free of charge via the Internet at http://pubs.acs.org.

JA9047043